Journal of Materials Chemistry A

Accepted Manuscript

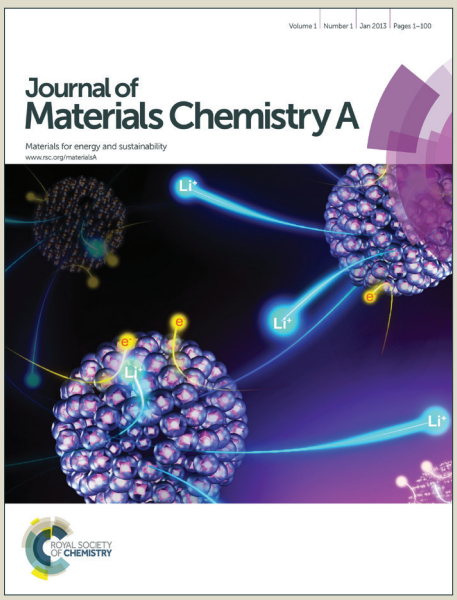

This is an *Accepted Manuscript*, which has been through the Royal Society of Chemistry peer review process and has been accepted for publication.

Accepted Manuscripts are published online shortly after acceptance, before technical editing, formatting and proof reading. Using this free service, authors can make their results available to the community, in citable form, before we publish the edited article. We will replace this *Accepted Manuscript* with the edited and formatted *Advance Article* as soon as it is available.

You can find more information about *Accepted Manuscripts* in the Information for Authors.

Please note that technical editing may introduce minor changes to the text and/or graphics, which may alter content. The journal's standard Terms & Conditions and the Ethical guidelines still apply. In no event shall the Royal Society of Chemistry be held responsible for any errors or omissions in this *Accepted Manuscript* or any consequences arising from the use of any information it contains.

ROYAL SOCIETY OF CHEMISTRY

www.rsc.org/materialsA

Tuning Electrochemical Performance of Si-Based Anodes for Lithium-ion Batteries by Employing Atomic Layer Deposition Alumina Coating

Ying Li, Yujie Sun, Guanjie Xu, Yao Lu, Shu Zhang, Leigang Xue, Jesse S. Jur, and Xiangwu Zhang*

Fiber and Polymer Science Program, Department of Textile Engineering, Chemistry and Science, North Carolina State University, Raleigh, NC 27695-8301, USA

* Corresponding author. Tel.: +1-919-515-6547; Fax: +1-919-515-6532.
E-mail address: xiangwu_zhang@ncsu.edu (X. Zhang)

Journal of Materials Chemistry A Accepted Manuscript

Abstract

Si-based anode materials were prepared by electrospinning and carbonization using polyacrylonitrile as the spinning medium and carbon precursor. The effects of atomic layer deposition (ALD) alumina coatings with different thicknesses on the electrochemical performance of Si/C composite nanofiber anodes were investigated. Results show that when the ALD alumina coating cycle number is 28, the capacity retention at 100th cycle increases significantly from 36.1% to 82.3% and the Columbic efficiency increases from 98.4% to 99.9%, compared to the uncoated Si/C nanofiber anode. This demonstrates the excellent stability of ALD alumina-coated Si/C composite nanofiber anodes. The enhanced electrochemical performance is mainly due to the protective effect of conformal ALD alumina coating, which could improve the mechanical integrity of the electrode structure and prevent the side reactions between the electrode and the electrolyte.

Keywords: Si nanoparticles, atomic layer deposition, electrospinning, carbon nanofibers, lithium-ion batteries, energy storage

Journal of Materials Chemistry A Accepted Manuscript

1. Introduction

Rechargeable batteries, particularly lithium-ion batteries (LIBs), have revolutionized the ubiquitous mobile electronic devices and attracted significant attention for being the potential power source for electric vehicles. In addition to broad operating temperature range, low self-discharge rate, no voltage depression, LIBs should also possess high energy density, long cycle life and excellent rate capability.[1-3] Among various anode materials, Si has the highest theoretical capacity (3579 mAh g^{-1}, corresponding to the formation of $Li_{15}Si_4$), which is about ten times higher than that of the commercially used graphite anode (372 mAh g^{-1}), and has been intensively studied for use in next-generation lithium-ion batteries.[2-5]

However, Si-based anode materials haven't made their way to the large-scale market mainly due to their rapid capacity fading, which is believed to be a result of both physical/mechanical failure and chemical degradation.[6,7] The physical/mechanical failure is generally induced by the huge volume change upon cycling, resulting in the loss of effective electrical contact and increased cell impedance. Chemical degradation is generally related to the formation of unstable electrode/electrolyte interface, which is commonly known as solid electrolyte interphase (SEI). The SEI film is mainly formed by the decomposed products of electrolyte solvents and salts, such as hydrocarbons, lithium alkyl carbonates, LiOH, Li_2CO_3, and other salt moieties like LiF for $LiPF_6$-based electrolytes.[8,9] In general, the SEI film is proportional to the surface area. As a result, the physical/mechanical failure could cause new SEI formation by creating larger surface area. This in turn results in larger irreversible capacity. Therefore, to improve the

Journal of Materials Chemistry A Accepted Manuscript

reversible capacity and cyclability of Si-based electrode materials, it is important to control both the structural stability and interfacial properties.

In order to overcome the drawbacks of Si-based electrode materials, many approaches have been proposed: 1) minimizing the cracking and pulverization of Si materials by employing various nanoscale electrode materials, like Si nanowire, [10-12] Si nanotube,[13,14] etc.; 2) introducing buffer and conductive phase, for example, dispersing Si into inactive/active matrices;[15-17] 3) employing new binder materials, such as synthetic and bio-derived polymers that contain carboxy groups,[18] conductive binders,[19] etc.; 4) improving the structure integrity and conductivity by using different surface modification methods, such as carbon coating,[20] metal coating,[21,22] etc.; 5) facilitating the formation of stable SEI film by employing different electrolyte additives;[23-25] and 6) controlling the cycling conditions of the battery.[26]

Among many surface modification methods, atomic layer deposition (ALD) has been known for its ability to provide ultrathin and conformal coating layers.[27-29] Recently, ALD coating has been shown as an effective way to improve the electrochemical performance of both cathodes and anodes.[30-34] In this work, we improved the conductivity of Si-based anodes by incorporating Si into an electrically-conductive carbon nanofiber matrix and enhanced the electrode integrity by employing ALD alumina coatings with different thicknesses. A free-standing, conductive and three-dimensional network of Si/C composite nanofibers was formed by electrospinning, which possesses good elasticity to maintain the structure integrity and stable electric conductive network.[35,36] ALD alumina coating acts as an artificial SEI to stabilize the electrode surface and prevent the side reaction during cycling. In addition, ALD alumina coating can further prevent Si

Journal of Materials Chemistry A Accepted Manuscript

composite nanofiber anodes from mechanical failure and loss of effective electronic contact.

2. Experimental

2.1 Electrode preparation

Si nanoparticles (diameter: 30 - 50 nm) were purchased from Nanostructured & Amorphous Materials, Inc. Polyacrylonitrile (PAN, 150,000 g mol^{-1}) was purchased from Pfaltz & Bauer Inc, and was used as the spinning media and carbon source. N,N-dimethylformamide (DMF) solvent was purchased from Aldrich. Trimethyaluminum (TMA, 98% purity, STREM chemical) and water (Sigma Aldrich, CAS No. 7732-18-5) were used as the alumina precursor in the ALD process. All these reagents were used without further purification.

The electrospinning dispersions were prepared by adding 15 wt % Si nanoparticles into 8 wt.% PAN solutions in DMF, and were stirred at 60 °C for 24 h, followed by ultrasonic treatment for 1 h. During electrospinning, a variable high voltage power supply (Gamma ES40P-20W/DAM) was used to provide a high voltage (18 kV). The flow rate used was 0.75 mL h^{-1} and the needle-to-collector distance was set as 15 cm. Electrospun fibers were collected on an aluminum foil. Electrospun Si/PAN composite nanofibers were stabilized in air environment at 280 ^{o}C for 5 h with a heating rate of 5 ^{o}C min^{-1} and then carbonized at 800 ^{o}C for 2 h in an argon atmosphere with a heating rate of 2 ^{o}C min^{-1} to form Si/C composite nanofibers. Elemental analysis (Perkin-Elmer, CHN 2400) of Si/C composite nanofibers showed that the Si-to-C ratio was 0.55.

Journal of Materials Chemistry A Accepted Manuscript

ALD Al_2O_3 coating was performed in a custom hot wall, flow tube reactor system. TMA and water were introduced into the chamber through the entrainment of nitrogen. The temperature used was 120 ^oC. Typical ALD cycle times were $TMA/N_2/H_2O/N_2$ = 0.2/30/0.2/45s. Since the ALD process has a self-limiting growth mechanism, the amount of sample has no effect on the ALD cycle as long as the precursor flux is large enough to saturate the substrate surface. The thickness of Al_2O_3 coating was hence controlled by ALD cycle numbers.

2.2 Nanofiber characterization

The morphology of Si/C and ALD Al_2O_3-coated Si/C composite nanofibers was examined by field emission scanning electron microscope (FESEM-JEOL 6400F SEM at 5 kV). The microstructure of Al_2O_3-coated Si/C composite nanofibers was observed using transmission electron microscope (Hitachi HF2000 TEM at 200 kV). The structure of composite nanofibers was also investigated by wide-angle X-ray diffraction (WAXD, Philips X'Pert PRO MRD HR X-Ray Diffraction System) and X-ray photoelectron spectroscopy (XPS, SPECS System with PHOIBOS 150 Analyzer). The composition of the resultant Al_2O_3-coated Si/C composite nanofibers was investigated by atomic resolution elemental mapping in scanning transmission electron microscope (S/TEM – FEI Titan 80-300) as well. The elemental mapping showed that the weight ratios of C, O, Al and Si of Al_2O_3-coated Si/C composite nanofibers prepared with 28 ALD cycles were 45.19, 4.65, 12.56 and 37.60 wt.%, respectively. The Si content measured by the elemental mapping technique cannot be compared directly with that obtained by the Elemental analysis (Perkin-Elmer, CHN 2400) method since there was a variation in the measured Si content values when two different methods were used.

Journal of Materials Chemistry A Accepted Manuscript

2.3 Electrochemical measurements

Both Si/C and Al_2O_3-coated Si/C composite nanofibers formed free-standing conductive membranes, and they were used directly as the working electrode in CR2032-type coin cells. The mass loading of active material in the working electrode was in the range of 2 – 3 mg cm^{-2}. Lithium metal was used as the counter electrode and Celgard 2400 membrane as the separator. The electrolyte used consisted of a 1 M solution of $LiPF_6$ dissolved in ethylene carbonate (EC)/diethyl carbonate (DEC)/dimethyl carbonate (DMC) (1/1/1, v/v/v). Electrochemical impedance spectra (EIS) were obtained using the Gamry Reference 600 Potentiostat/Galvanostat/ZRA with a 10.0 mV AC voltage signal in the 10^6 - 10^{-2} Hz frequency range. Before EIS measurements, the electrodes were first charged galvanostatically at 50 mAg^{-1} to 0.01 V, and then remained at open circuit for 5.0 h to allow their potential to stabilize. The electrochemical performance was investigated by carrying out galvanostatic charge-discharge experiments at different current densities between cut-off potentials of 0.01 and 1.5 V. The capacity was calculated based on the total weight of Si nanoparticles and carbon nanofibers since Li^+ can also intercalate into the carbon matrix.[35] In order to understand the protective effect of the ALD Al_2O_3 coating and impact of cycling on the composite nanofiber structure, the morphology change of composite nanofibers after 100 cycles was examined by FESEM.

The reproducibility of electrochemical results was ensured by conducting all measurements on at least six cells for each composite nanofiber sample.

Journal of Materials Chemistry A Accepted Manuscript

3. Results and discussion

3.1 Morphology and structure of Al_2O_3-coated Si/C composite nanofibers

Figure 1 shows a schematic diagram of the synthesis procedure of Al_2O_3-coated Si/C composite nanofibers. Si/C composite nanofibers were obtained via electrospinning and carbonization. After carbonization, the formed Si/C composite nanofibers were coated with a conformal layer of Al_2O_3 coating. The thickness of the deposited Al_2O_3 coating was tuned at monolayer-scale via adjusting the number of ALD cycles. The pristine Si/C composite has Si nanoparticles either embedded inside the nanofibers or exposed on the surface. During charge-discharge cycling, the exposed Si nanoparticles on uncoated Si/C composite nanofibers can form heavy solid electrolyte interface (SEI) and often fall off from the nanofiber network upon repeat cycling. In contrast, the ALD coating layer on the Si/C composite nanofiber surface can help stabilize the SEI and protect the integrity of the electrode.

Figure 2 shows the XRD patterns of Si nanoparticles, Si/C composite nanofibers, and Al_2O_3-coated Si/C composite nanofibers. It is seen that Si nanoparticles show clear diffractions at 28.4^o, 47.4^o, 56.2^o, 69.2^o, 76.5^o and 88.1^o, which are corresponded to the (111), (220), (311), (400), (331) and (422) planes of crystalized Si, respectively. After incorporating Si nanoparticles into the carbon matrix, the resultant Si/C composite nanofibers exhibit the same Si peaks, but with lower intensities. A similar XRD pattern is also obtained for the Al_2O_3-coated Si/C composite nanofibers but with even lower intensities. No peaks can be found for silicon oxide or Si-C alloy, indicating that Si was not oxidized or did not react with carbon during the carbonization and ALD processes.[37,38] One new peak around 25^o can be found for Si/C and Al_2O_3-coated Si/C

Journal of Materials Chemistry A Accepted Manuscript

nanofibers due to the formation of carbon nanofiber matrix. However, the peak is weak and broad, indicating that the carbon matrix is mainly composed of disordered carbon. Comparing curves b and c, it is seen that there is no apparent difference between XRD patterns of Si/C and Al_2O_3-coated Si/C composite nanofibers, indicating that the ALD Al_2O_3 coating is mainly formed by amorphous alumina.

The morphology of Si/C and Al_2O_3-coated Si/C composite nanofibers and their precursors were examined by SEM. Figures 3 compares typical SEM images of Si/PAN and Si/C composite nanofibers. The Si/PAN composite nanofibers appear continuous and form a 3-D intertwined fibrous mat. Si nanoparticles are distributed along the nanofibers, and some of the particles form clusters on the fiber surface. The diameters of Si/PAN composite nanofibers are in the range of 150 to 300 nm. After carbonization, the as-spun Si/PAN composite nanofibers are converted into Si/C nanofibers and the diameter of nanofibers are reduced. Compared with the corresponding Si/PAN precursor shown in Figures 3A, Si/C composite nanofibers have more Si nanoparticles exposed on the surface. The presence of free space around the entangled Si/C nanofibers allows the formation of a porous network through which Li^+ ions can migrate easily and reach all Si/C composite nanofiber surfaces. The 3-D interconnected network is also beneficial for structure stability due to the ability of absorbing the mechanical stress induced by repeat cycling.

Figure 4 displays the morphology of Al_2O_3-coated Si/C composite nanofibers with different ALD cycle numbers. The coating thickness was controlled by ALD cycles, and a higher cycle number indicates a thicker coating. From Figure 4, it can be seen that in all samples, both the fibers and exposed Si nanoparticles are coated with bright shells

Journal of Materials Chemistry A Accepted Manuscript

corresponding to the Al_2O_3 coatings. These results confirm that the original 3-D morphology and network of Si/C composite nanofibers were preserved during the successive ALD processing cycles.

EDX elemental mapping was employed to further identify the existence and uniformity of ALD Al_2O_3 coating. Figure 5 shows the EDX elemental mapping images for C, Si, Al, and O elements. From the C and Si element mappings, it is seen that some Si nanoparticles are wrapped completely inside the carbon nanofiber matrix and some Si nanoparticles are partly exposed on the nanofiber surface. From the Al element mapping, it is seen that the fiber boundary is very clear, which confirms the ALD Al_2O_3 coating is desirably limited on the exposed Si nanoparticle surface and the nanofiber surface layer. Furthermore, the EDX mapping reveals the uniform distribution of Al and O elements on the Si/C composite nanofibers, which indicates that the ALD Al_2O_3 coating completely covers the surface of Si/C composite nanofibers.

TEM was employed to investigate the detailed microscopic structure of Al_2O_3-coated Si/C composite nanofibers, and the results are shown in Figure 6. It is seen that most of Si particles are encapsulated in the fibers and some Si particles are dispersed on the fiber surface forming agglomerates. For all samples, the surfaces of composite nanofibers are uniformly covered by ALD Al_2O_3 coatings. More importantly, for the Si particles partly embedded in the nanofibers, the exposed Si surfaces are coated by homogeneous ALD Al_2O_3 coating layers. Average thicknesses of ALD Al_2O_3 coating layers were evaluated by measuring 10 different areas for each sample, and results show that the coating thickness increases from 2 nm to 10 nm when the ALD cycle number increases from 7 to 35. In addition, the ALD Al_2O_3 coating layers do not present any

Journal of Materials Chemistry A Accepted Manuscript

ordered structure, which is in agreement with the XRD analysis. Generally, the structure stability of composite nanofiber anodes is diminished by the partly embedded Si nanoparticles and Si agglomerates when under repeat volume changes.[35,39,40] However, in this work, the ALD Al_2O_3 coating can help maintain the structure integrity and mitigate capacity fading. At the same time, the ALD Al_2O_3 coating may act as an artificial SEI film to stabilize the electrode surface and prevent undesirable side reactions during cycling.

Figure 7 shows XPS spectra of Si/C nanofibers and Al_2O_3-coated Si/C nanofibers after the first charge-discharge cycle. No interaction between Al_2O_3 coating and Si/C nanofibers can be observed. From Figure 7, it is also seen that the intensity of the LiF peak (around 685 eV) of Al_2O_3-coated Si/C composite nanofibers is lower than that of Si/C composite nanofibers, indicating that the ALD Al_2O_3 coating prohibits the decomposition of $LiPF_6$ on the electrode surface. The effects of ALD Al_2O_3 coating on the electrochemical performance of Si/C composite nanofiber anodes are discussed in the following sections.

3.2 Electrochemical performance of Al_2O_3-coated Si/C composite nanofibers

Figure 8A displays the impedance spectra of Si/C and ALD Al_2O_3-coated Si/C composite nanofibers with different ALD cycle numbers. It is seen that these EIS spectra show one or two depressed semicircles in the high and intermediate frequency range and a straight line in the low frequency range, corresponding to the formation of SEI film, interfacial charge transfer process, and lithium diffusion in the electrode, respectively.[41,42] Figure 8B shows the corresponding equivalent circuit. Here, R_e represents the electrolyte

Journal of Materials Chemistry A Accepted Manuscript

resistance of the cell, R_{sl} is the resistance of ions transferring through the surface layer in the high frequency range, and R_{ct} is the charge transfer resistance in intermediate frequency region. Warburg impedance (W) stands for the diffusion process of lithium ions within the electrode in the low frequency range.[9,42] In general, the ionic conduction of the SEI film is a result of the migration of solvated Li ions through the micro-pores of SEI since the dried SEI itself is neither electronic conductive nor ionic conductive.[8,9,42] Hence, higher interfacial resistance corresponds to a more compact and more stable SEI. As shown in Figure 8A, the fitted impedance curves indicated by solid lines agree well with the actual impedance data. The obtained R_{sl} and R_{ct} values are listed in Table 1. The diameter of the nanofiber electrodes was 0.5 inch. It is seen that the R_{sl} value of Al_2O_3-coated Si/C composite nanofibers with 0, 7, 14, 21, 28 and 35 ALD cycles is 25.29, 26.76, 29.33, 38.49, 63.49 and 90.74 ohm, respectively. The R_{ct} value of Al_2O_3-coated Si/C composite nanofibers with 0, 7, 14 and 21 ALD cycles are comparable and are between 76.72 and 78.91 ohm. When the ALD cycle number increases to 28, the R_{ct} value increases slightly to 83.67 ohm. When the ALD cycle number further increases to 35, the R_{ct} value shows a significant increase and reaches 105.68 ohm, compared to that of uncoated Si/C composite nanofibers. This indicates that the SEI structure has become more compact and less conductive due to ALD Al_2O_3 coating.

Galvanostatic charge-discharge tests were carried out at a current density of 50 mA g^{-1} within a voltage window of 0.02 – 1.5 V to evaluate the electrochemical performance of Si/C and Al_2O_3-coated Si/C composite nanofiber anodes. Figure 9A shows galvanostatic charge-discharge curves of Si/C and Al_2O_3-coated Si/C composite nanofibers under 50 mA g^{-1}. When the ALD coating cycle number is 35, the resultant

Journal of Materials Chemistry A Accepted Manuscript

Al_2O_3-coated Si/C composite nanofibers exhibit no useful capacity. This means that an Al_2O_3 coating layer of 35 ALD cycles is too thick and blocks the lithium diffusion, which is in agreement with the EIS result. As shown in Figure 9A, all other uncoated and Al_2O_3-coated Si/C composite nanofibers show reversible capacities of greater than 900 mAh/g in the first cycle.

Figure 9B shows the cycling performance of uncoated and Al_2O_3-coated Si/C composite nanofibers. It is seen that at the 100th cycle, the discharge capacities are 338.8, 378.8, 473.5, 685.1 and 827.3 mAh g^{-1}, respectively, for composite nanofibers with 0, 7, 14, 21, and 28 ALD cycles. The corresponding capacity retentions are 36.1, 39.8, 47.4, 66.5 and 82.3%, respectively. When the ALD coating cycle number is 7 or 14, the cycling performance of Al_2O_3-coated Si/C nanofibers is comparable to that of the uncoated Si/C nanofibers. When the ALD coating cycle number is 21, the capacity fades slower than that of uncoated Si/C nanofibers and shows an increased capacity retention of 66.5% at the 100th cycle. When the ALD coating cycle number is 28, the capacity exhibits the highest stability and the capacity retention at the 100th cycle increases significantly from 36.1% to 82.3%, compared to that of uncoated Si/C nanofibers. However, when the ALD coating cycle number further increases to 35, the capacity is lower than 200 mAh g^{-1} and fades very quickly. These results demonstrate that Al_2O_3-coated Si/C composite nanofibers prepared with an ALD cycle number of 28 have the most stable cycling performance. The enhanced cycling performance is mainly due to the protective effect of conformal ALD alumina coating which could improve the mechanical integrity and prevent the side reactions between the electrode and the electrolyte. To achieve the enhanced cycling performance, it is important to select an appropriate ALD

Journal of Materials Chemistry A Accepted Manuscript

Al_2O_3 coating thickness, which is a critical parameter for determining the electrochemical performance of the Al_2O_3-coated composite nanofibers.

Figure 9C compares of the Columbic efficiencies of Si/C and Al_2O_3-coated Si/C composite nanofiber anodes during cycling. It is seen that Al_2O_3-coated Si/C composite nanofibers prepared with 28 ALD cycles deliver the highest Columbic efficiency of 99.9% at the 100th cycle, corresponding to a 1.5% point improvement, compared to that of uncoated Si/C composite nanofibers. By adjusting the ALD cycles, the Columbic efficiency of Al_2O_3-coated Si/C composite nanofibers is higher than that of Si nanoparticles and nanowires reported in literature.[4,11] Similar to the enhanced cycling performance, the improved Columbic efficiency can be mainly attributed to the ultrathin conformal ALD Al_2O_3 coating, which minimizes the side reactions between the electrode and the electrolyte.

In order to understand the impact of cycling on the composite nanofiber structure, the morphology change of composite nanofibers after 100 cycles was analyzed. As shown in Figure 10, uncoated Si/C composite nanofibers exhibit a film-like morphology with many cracks, which could reduce the electronic conduction and the buffer effect of carbon nanofiber matrix, resulting in large capacity fading during cycling. On the other hand, Al_2O_3-coated Si/C composite nanofibers keep regular fibrous structure and relatively homogeneous morphology. This further indicates that ALD Al_2O_3 coating acts as a protective layer and helps prevent Si composite nanofibers from mechanical failure and loss of effective electronic contact.

Journal of Materials Chemistry A Accepted Manuscript

ALD Al_2O_3 coating tunes the electrochemical performance of Si-based anode materials from both physical and chemical aspects, as shown in Figure 11. Firstly, the ALD Al_2O_3 coating has strong physical/mechanical restrain effect on the Si/C composite nanofibers since the coating might transfer the stress of Si nanoparticle expansion from radial direction to in-plane restrain when the Si nanoparticle is partly exposed on the surface. As a result, due to the presence of disordered carbon structure or voids, the buffer effect of carbon matrix could be well realized by restricting the expansion of silicon to the carbon nanofiber (Figure 11A). Secondly, the ALD Al_2O_3 coating may act as a barrier for further side reactions between the electrode and the electrolyte (Figure 11B). The role of a chemical barrier combined with the reasonable mechanical properties makes the Al_2O_3 coating an artificial but strong and stable structure to improve the cycling performance and Columbic efficiency of Si-based anode.

In addition to improving the mechanical integrity of the electrode structure and preventing the side reactions between the electrode and the electrolyte, other structure parameters are also important in determining the overall performance of Si/C composite nanofiber anodes. In this work, the volumetric capacity of Al_2O_3-coated Si/C composite nanofibers prepared with 28 ALD cycles is around 110 mAh/cm^3, which is relatively low for practical application. To increase high volumetric capacity, the nanofiber electrodes can be compressed to reduce their porosity and increase their density by introducing a hot pressing or calendaring step before carbonization. This should also be one focus of future development work.

4. Conclusions

Journal of Materials Chemistry A Accepted Manuscript

In this work, the effects of ALD Al_2O_3 coatings with different thicknesses on the electrochemical performance of Si/C composite nanofiber anodes were investigated. Results show that when the ALD alumina coating cycle number is 28, the electrode show the best electrochemical performance. After 100 cycles, the capacity retention increases significantly from 36.1% to 82.3% and the Columbic efficiency increases from 98.4% to 99.9%, compared to the uncoated Si/C nanofiber anode. This demonstrates the excellent stability of Al_2O_3-coated Si/C composite nanofiber anodes. The enhanced cycling performance and Columbic efficiency are mainly due to the protective effect of conformal ALD Al_2O_3 coating which could improve the mechanical integrity of the electrode structure and prevent the side reactions between the electrode and the electrolyte. This indicates that tuning the anode electrochemical performance for lithium-ion batteries by employing atomic layer deposition might provide new opportunities for the battery industry to design other novel nanostructured electrodes that are highly durable.

Acknowledgements

This research was supported by the U.S. Department of Energy under Grant No: DE-EE0001177, Advanced Transportation Energy Center, and ERC Program of the National Science Foundation under Award Number EEC-08212121.

Journal of Materials Chemistry A Accepted Manuscript

References

1. B. Dunn, H. Kamath, and J. M. Tarascon, *Science*, 2011, **334**, 928–935.
2. M. Armand and J. M. Tarascon, *Nature*, 2008, **451**, 652–657.
3. J. M. Tarascon and M. Armand, *Nature*, 2001, **414**, 359–367.
4. M. N. Obrovac and L. J. Krause, *J. Electrochem. Soc.*, 2007, **154**, A103.
5. M. N. Obrovac and L. Christensen, *Electrochem. Solid-State Lett.*, 2004, **7**, A93.
6. P. Arora, R. E. White, and M. Doyle, *J. Electrochem. Soc.*, 1998, **145**, 3647–3667.
7. J. Vetter, P. Novák, M. R. Wagner, C. Veit, K. C. Möller, J. O. Besenhard, M. Winter, M. Wohlfahrt-Mehrens, C. Vogler, and A. Hammouche, *Journal of Power Sources*, 2005, **147**, 269–281.
8. S. Zhang, M. S. Ding, K. Xu, J. Allen, and T. R. Jow, *Electrochem. Solid-State Lett.*, 2001, **4**, A206.
9. K. Xu, S. Zhang, and T. R. Jow, *Electrochem. Solid-State Lett.*, 2003, **6**, A117.
10. L.-F. Cui, Y. Yang, C.-M. Hsu, and Y. Cui, *Nano Lett.*, 2009, **9**, 3370–3374.
11. C. K. Chan, H. Peng, G. Liu, K. McIlwrath, X. F. Zhang, R. A. Huggins, and Y. Cui, *Nature Nanotechnology*, 2007, **3**, 31–35.
12. C. K. Chan, R. N. Patel, M. J. O'Connell, B. A. Korgel, and Y. Cui, *ACS Nano*, 2010, **4**, 1443–1450.
13. M.-H. Park, M. G. Kim, J. Joo, K. Kim, J. Kim, S. Ahn, Y. Cui, and J. Cho, *Nano Lett.*, 2009, **9**, 3844–3847.
14. L. Hu, H. Wu, Y. Gao, A. Cao, H. Li, J. McDough, X. Xie, M. Zhou, and Y. Cui, *Adv. Energy Mater.*, 2011, **1**, 523–527.
15. L. Ji, K.-H. Jung, A. J. Medford, and X. Zhang, *J. Mater. Chem.*, 2009, **19**, 4992.

Journal of Materials Chemistry A Accepted Manuscript

16. G. Jeong, Y.-U. Kim, S. A. Krachkovskiy, and C. K. Lee, *Chem. Mater.*, 2010, **22**, 5570–5579.

17. Y. Li, G. Xu, L. Xue, S. Zhang, Y. Yao, Y. Lu, O. Toprakci, and X. Zhang, *J. Electrochem. Soc.*, 2013, **160**, A528–A534.

18. I. Kovalenko, B. Zdyrko, A. Magasinski, B. Hertzberg, Z. Milicev, R. Burtovyy, I. Luzinov, and G. Yushin, *Science*, 2011, **334**, 75–79.

19. G. Liu, S. Xun, N. Vukmirovic, X. Song, P. Olalde-Velasco, H. Zheng, V. S. Battaglia, L. Wang, and W. Yang, *Adv. Mater.*, 2011, **23**, 4679–4683.

20. S. H. Ng, J. Wang, D. Wexler, S. Y. Chew, and H. K. Liu, *J. Phys. Chem. C*, 2007, **111**, 11131–11138.

21. S. Murugesan, J. T. Harris, B. A. Korgel, and K. J. Stevenson, *Chem. Mater.*, 2012, **24**, 1306–1315.

22. Y. Yu, L. Gu, C. Zhu, S. Tsukimoto, P. A. van Aken, and J. Maier, *Adv. Mater.*, 2010, **22**, 2247–2250.

23. Y. Li, G. Xu, Y. Yao, L. Xue, S. Zhang, Y. Lu, O. Toprakci, and X. Zhang, *J Solid State Electrochem*, 2013, 1–7.

24. L. Chen, K. Wang, X. Xie, and J. Xie, *Journal of Power Sources*, 2007, **174**, 538–543.

25. S. Dalavi, P. Guduru, and B. L. Lucht, *J. Electrochem. Soc.*, 2012, **159**, A642.

26. Q. Si, K. Hanai, N. Imanishi, M. Kubo, A. Hirano, Y. Takeda, and O. Yamamoto, *Journal of Power Sources*, 2009, **189**, 761–765.

27. S. M. George, *Chem. Rev.*, 2010, **110**, 111–131.

28. M. Knez, K. Nielsch, and L. Niinistö, *Adv. Mater.*, 2007, **19**, 3425–3438.

Journal of Materials Chemistry A Accepted Manuscript

29. S. C. Jung and Y. K. Han, *J. Phys. Chem. Lett.*, **2013**, 4, 2681–2685.

30. H.-M. Cheng, F.-M. Wang, J. P. Chu, R. Santhanam, J. Rick, and S.-C. Lo, *J. Phys. Chem. C*, 2012, **116**, 7629–7637.

31. F.-F. Cao, J.-W. Deng, S. Xin, H.-X. Ji, O. G. Schmidt, L.-J. Wan, and Y.-G. Guo, *Adv. Mater.*, 2011, **23**, 4415–4420.

32. Y. S. Jung, A. S. Cavanagh, A. C. Dillon, M. D. Groner, S. M. George, and S.-H. Lee, *J. Electrochem. Soc.*, 2010, **157**, A75.

33. Y. S. Jung, A. S. Cavanagh, L. A. Riley, S.-H. Kang, A. C. Dillon, M. D. Groner, S. M. George, and S.-H. Lee, *Adv. Mater.*, 2010, **22**, 2172–2176.

34. Y. He, X. Yu, Y. Wang, H. Li, and X. Huang, *Adv. Mater.*, 2011, **23**, 4938–4941.

35. Y. Li, B. Guo, L. Ji, Z. Lin, G. Xu, Y. Liang, S. Zhang, O. Toprakci, Y. Hu, and M. Alcoutlabi, *Carbon*, 2013, **51**, 185–194.

36. Y. Li, Z. Lin, G. Xu, Y. Yao, S. Zhang, O. Toprakci, M. Alcoutlabi, and X. Zhang, *ECS Electrochemistry Letters*, 2012, **1**, A31–A33.

37. Z. P. Guo, E. Milin, J. Z. Wang, J. Chen, and H. K. Liu, *J. Electrochem. Soc.*, 2005, **152**, A2211.

38. A. M. Wilson and J. R. Dahn, *J. Electrochem. Soc.*, 1995, **142**, 326–332.

39. M. Gu, Y. Li, X. Li, S. Hu, X. Zhang, W. Xu, S. Thevuthasan, D. R. Baer, J.-G. Zhang, J. Liu, and C. Wang, *ACS Nano*, 2012, **6**, 8439–8447.

40. M. Alcoutlabi, J. Liwen, B. Guo, S. Li, Y. Li, S. Zhang, O. Toprakci, and X. Zhang, *AATCC Review: the magazine of the textile dyeing, printing, and finishing industry*, 2011, **11**, 45–51.

41. X. W. Zhang, P. K. Patil, C. Wang, A. J. Appleby, F. E. Little, and D. L. Cocke,

Journal of Materials Chemistry A Accepted Manuscript

Journal of Power Sources, 2004, **125**, 206–213.

42. K. Xu, *Chem. Rev.*, 2004, **104**, 4303–4418.

Journal of Materials Chemistry A Accepted Manuscript

Captions of Figures

Table1. AC impedance analysis results of Si/C composite nanofibers and Al_2O_3-coated Si/C composite nanofibers with different ALD cycle numbers. The diameter of the nanofiber electrodes was 0.5 inch.

Figure 1. Schematic of (A) Si/PAN composite nanofibers, (B) Si/C composite nanofibers, and (C) Al_2O_3-coated Si/C composite nanofibers.

Figure 2. XRD patterns of (a) Si, (b) Si/C composite nanofibers, and (c) Al_2O_3-coated Si/C composite nanofibers (ALD cycle number = 28).

Figure 3. SEM images of (A) Si/PAN composite nanofibers, and (B) Si/C composite nanofibers.

Figure 4. SEM images of Al_2O_3-coated Si/C composite nanofibers with different ALD cycle numbers: (A, B) 7, (C, D) 14, (E, F) 21, (G, H) 28, and (I, J) 35 cycles.

Figure 5. EDX elemental mapping of Al_2O_3-coated Si/C composite nanofibers (ALD cycle number = 28): (A) corresponded STEM image, (B) C element mapping, (C) Si element mapping, (D) Al element mapping, and (E) O element mapping.

Figure 6. TEM images of Al_2O_3-coated Si/C composite nanofibers with different ALD cycle numbers: (A, B) 7, (C, D) 14, (E, F) 21, (G, H) 28, and (I, J) 35 cycles.

Figure 7. XPS spectra (F1s) of Si/C composite nanofibers and Al_2O_3-coated Si/C composite nanofibers (ALD cycle number = 28) after the first charge-discharge cycle.

Journal of Materials Chemistry A Accepted Manuscript

Figure 8. (A) Nyquist plots and (B) equivalent circuit of Si/C composite nanofibers and Al_2O_3-coated Si/C composite nanofibers. In (A), symbols show experimental data and solid lines are fitted curves.

Figure 9. (A) Galvanostatic charge-discharge curves, (B) cycling performance, and (C) Columbic efficiencies of Si/C composite nanofibers and Al_2O_3-coated Si/C composite nanofibers.

Figure 10. SEM images of (A, B) Si/C composite nanofibers and (C, D) Al_2O_3-coated Si/C composite nanofibers (ALD cycle number = 28) after 100 charge-discharge cycles at a constant current density of 50 mA g^{-1}.

Figure 11. Schematic of (A) Physical/Mechanical, (B) Chemical protective effect.

Journal of Materials Chemistry A Accepted Manuscript

Table1. AC impedance analysis results of Si/C composite nanofibers and Al_2O_3-coated Si/C composite nanofibers with different ALD cycle numbers. The diameter of the nanofiber electrodes was 0.5 inch.

Electrodes	R_{sl} (ohm)	R_{ct} (ohm)
Si/C	25.29	76.72
7 cycles	26.76	79.25
14 cycles	29.33	78.41
21 cycles	38.49	78.91
28 cycles	63.79	83.67
35 cycles	90.74	105.68

Journal of Materials Chemistry A Accepted Manuscript

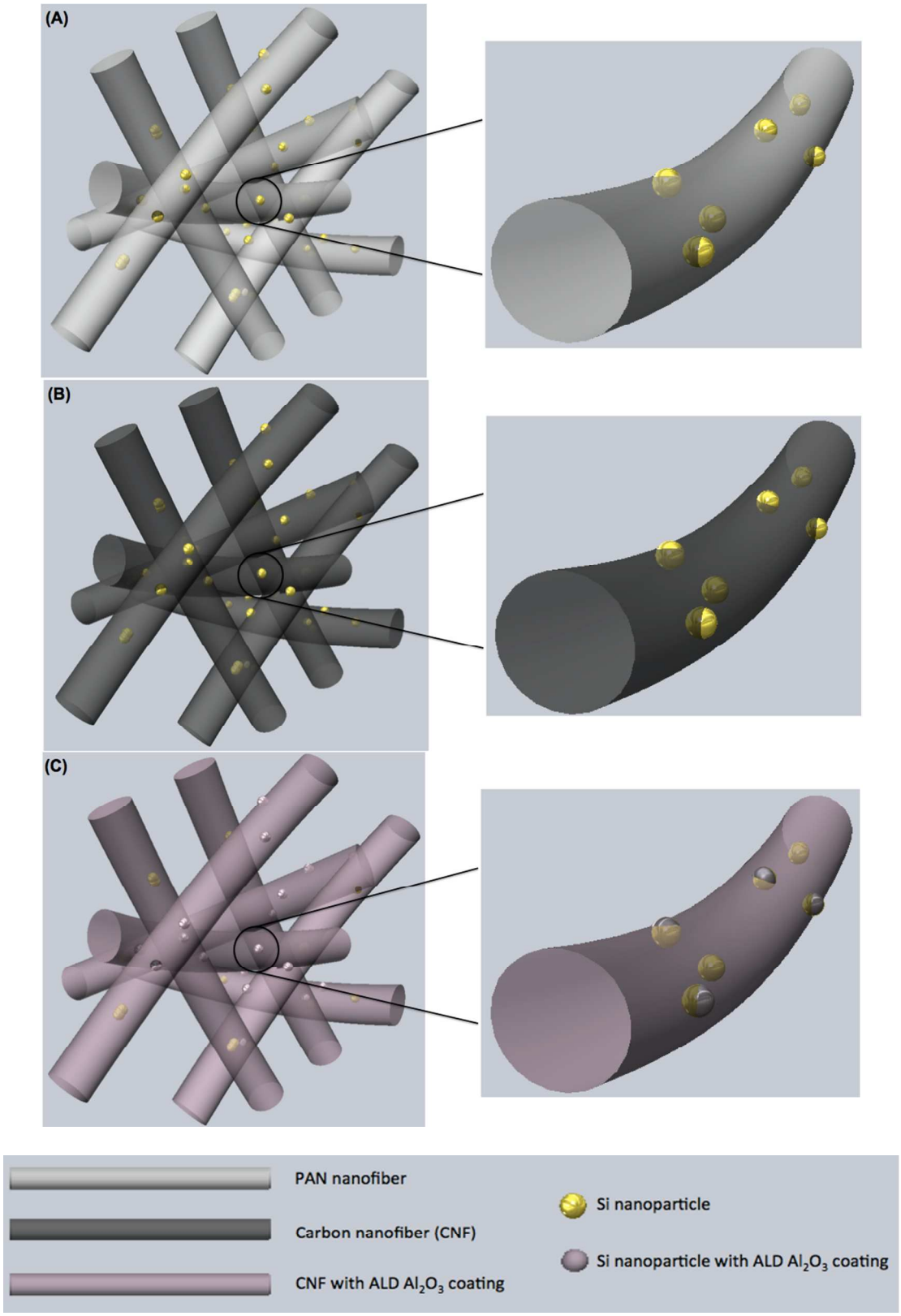

Figure 1. Schematic of (A) Si/PAN composite nanofibers, (B) Si/C composite nanofibers, and (C) Al_2O_3-coated Si/C composite nanofibers.

Journal of Materials Chemistry A Accepted Manuscript

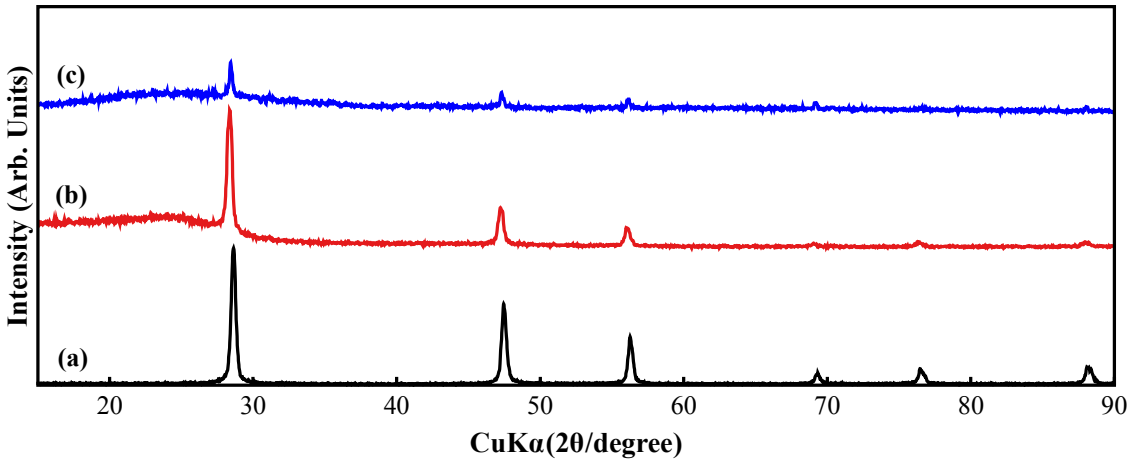

Figure 2. XRD patterns of (a) Si, (b) Si/C composite nanofibers, and (c) Al_2O_3-coated Si/C composite nanofibers (ALD cycle number = 28).

Journal of Materials Chemistry A Accepted Manuscript

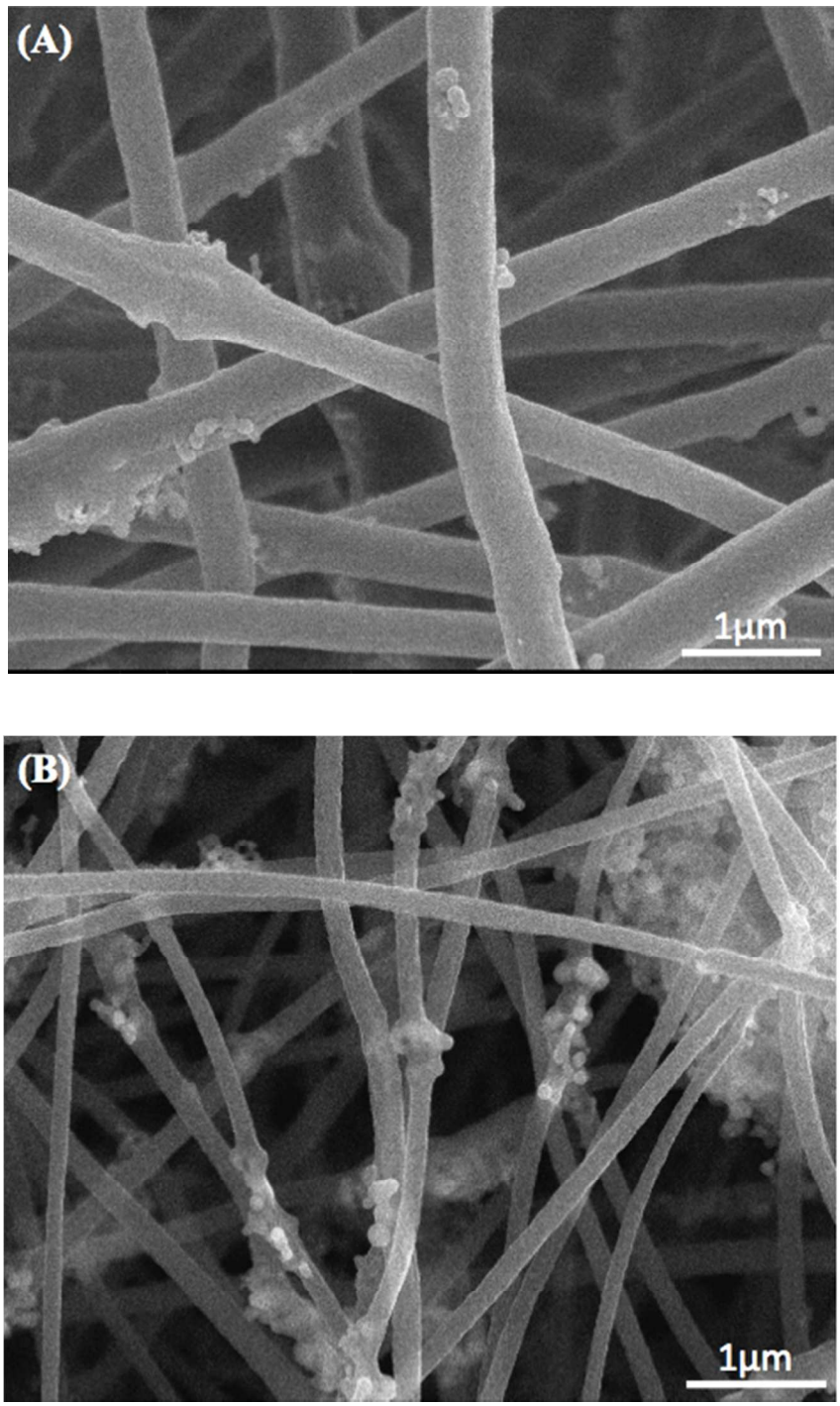

Figure 3. SEM images of (A) Si/PAN composite nanofibers, and (B) Si/C composite nanofibers.

Journal of Materials Chemistry A Accepted Manuscript

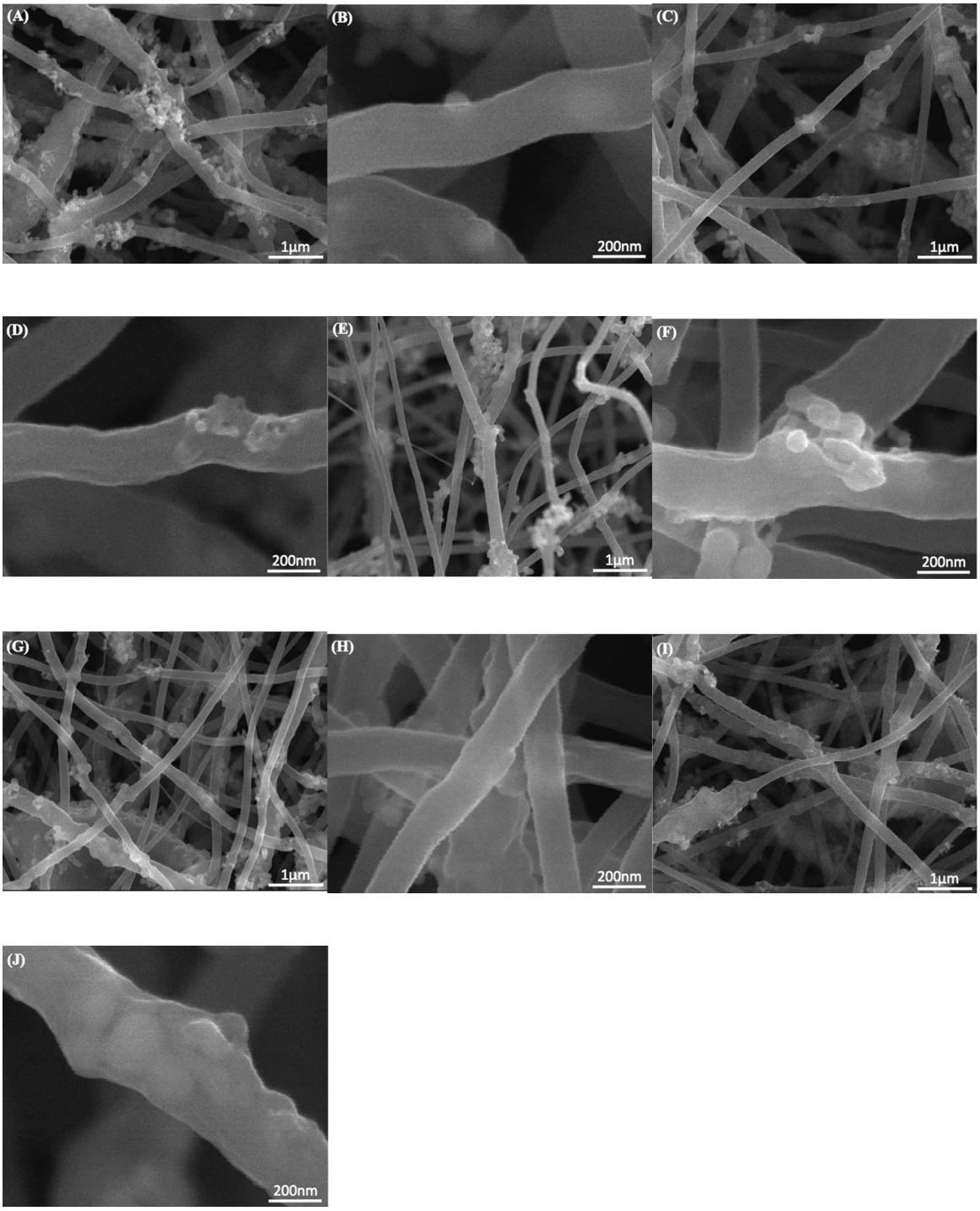

Figure 4. SEM images of Al_2O_3-coated Si/C composite nanofibers with different ALD cycle numbers: (A, B) 7, (C, D) 14, (E, F) 21, (G, H) 28, and (I, J) 35 cycles.

Journal of Materials Chemistry A Accepted Manuscript

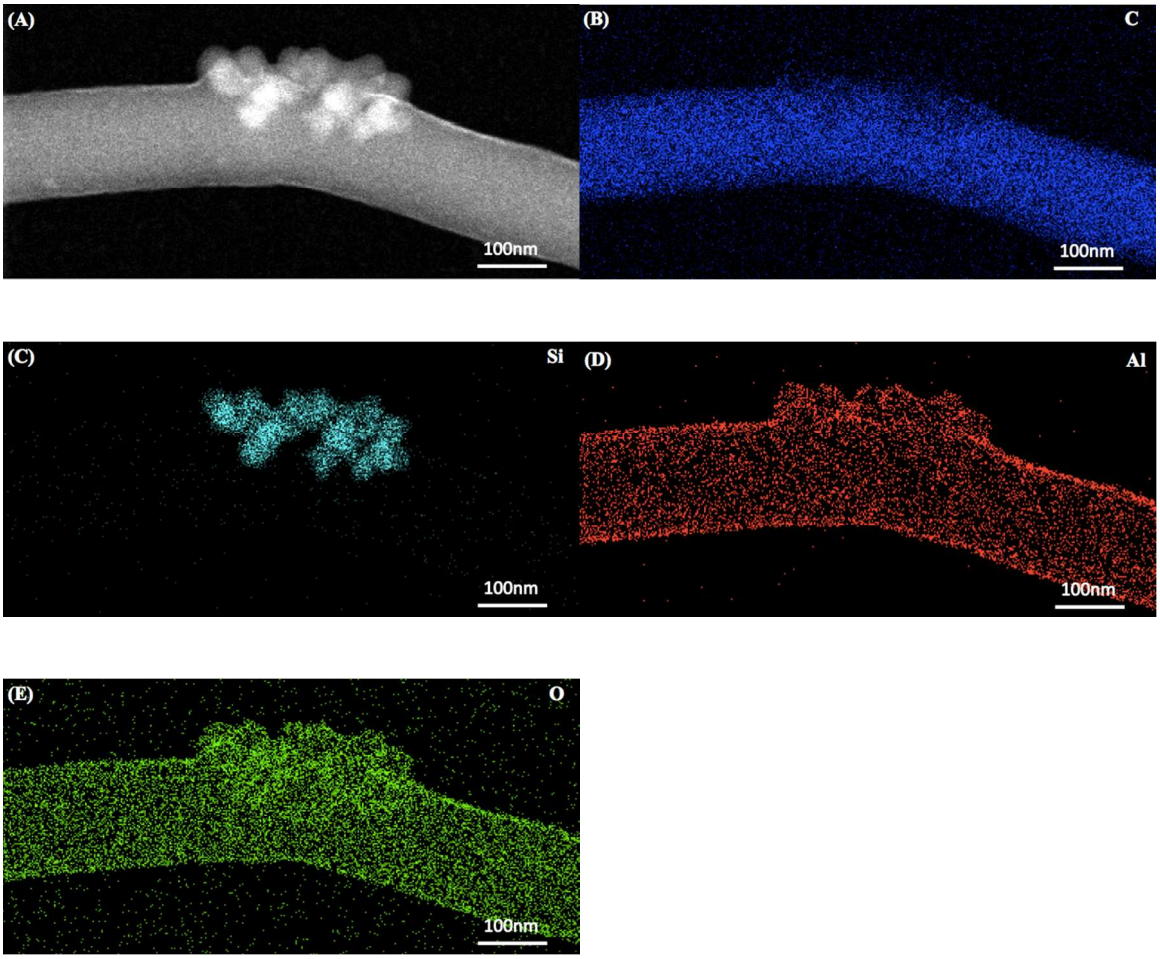

Figure 5. EDX elemental mapping of Al_2O_3-coated Si/C composite nanofibers (ALD cycle number = 28): (A) corresponded STEM image, (B) C element mapping, (C) Si element mapping, (D) Al element mapping, and (E) O element mapping.

Journal of Materials Chemistry A Accepted Manuscript

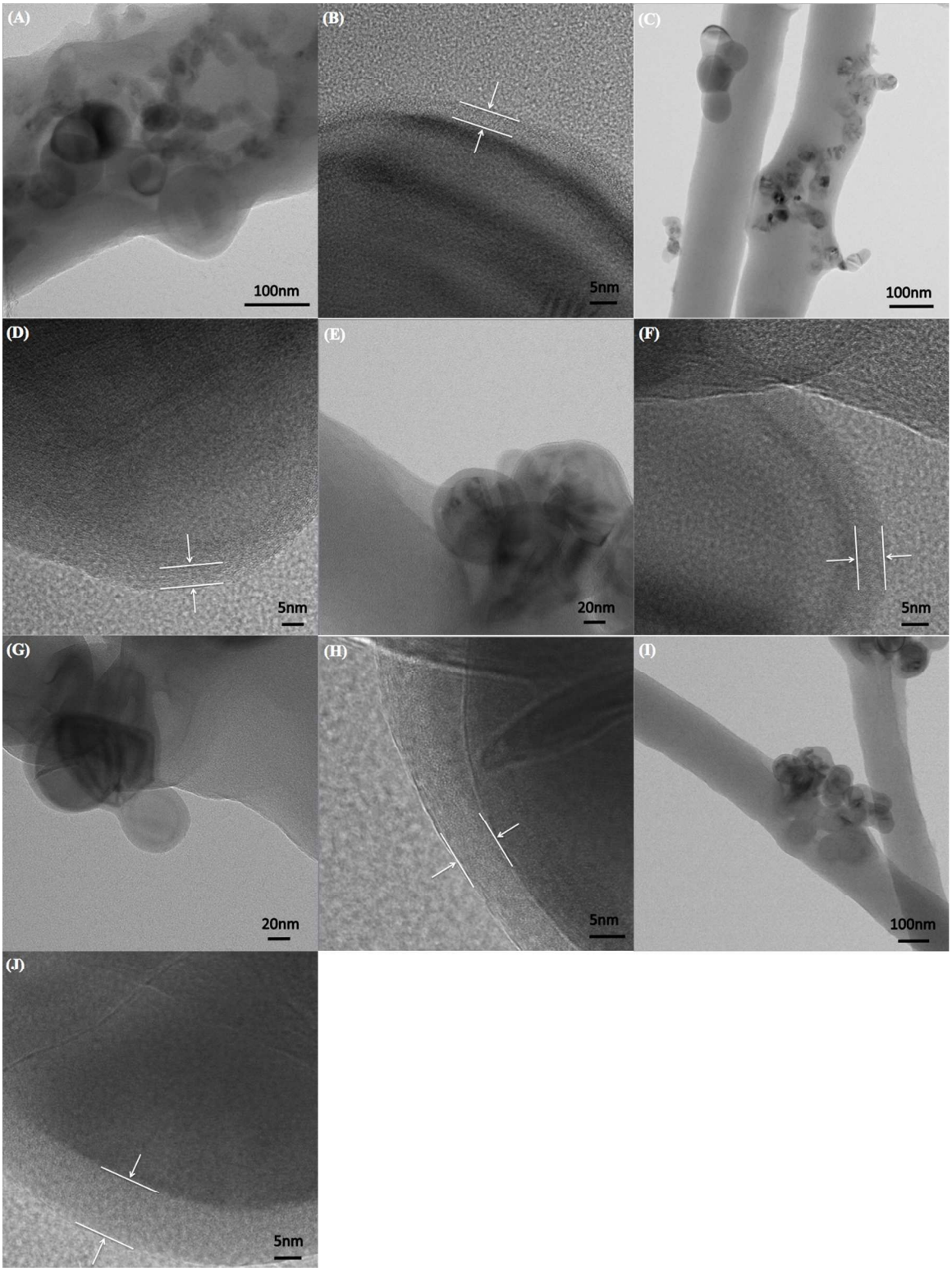

Figure 6. TEM images of Al_2O_3-coated Si/C composite nanofibers with different ALD cycle numbers: (A, B) 7, (C, D) 14, (E, F) 21, (G, H) 28, and (I, J) 35 cycles.

Journal of Materials Chemistry A Accepted Manuscript

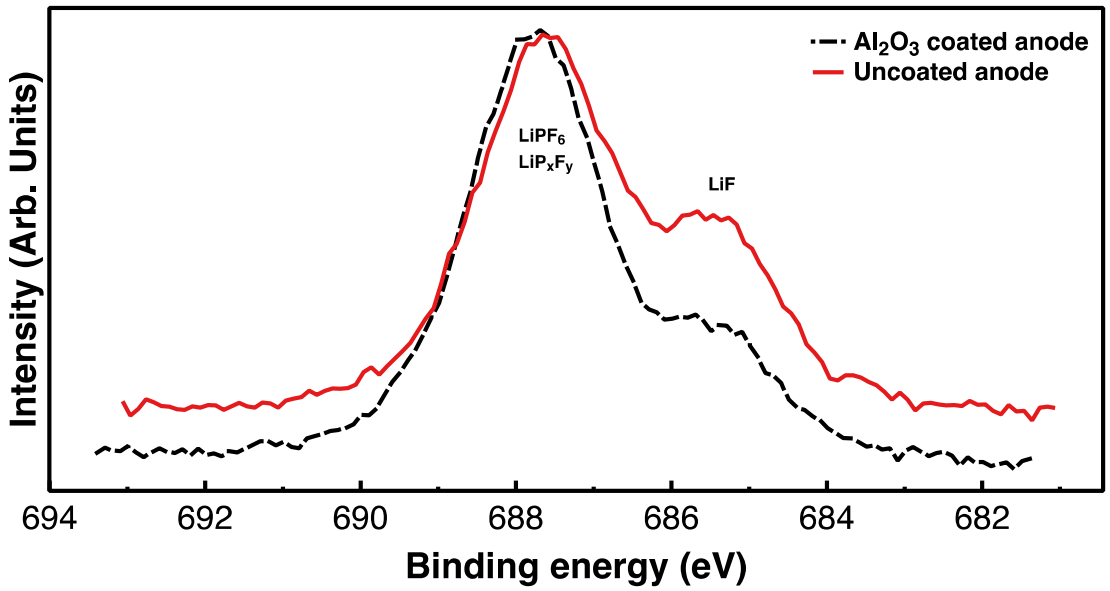

Figure 7. XPS spectra (F1s) of Si/C composite nanofibers and Al_2O_3-coated Si/C composite nanofibers (ALD cycle number = 28) after the first charge-discharge cycle.

Journal of Materials Chemistry A Accepted Manuscript

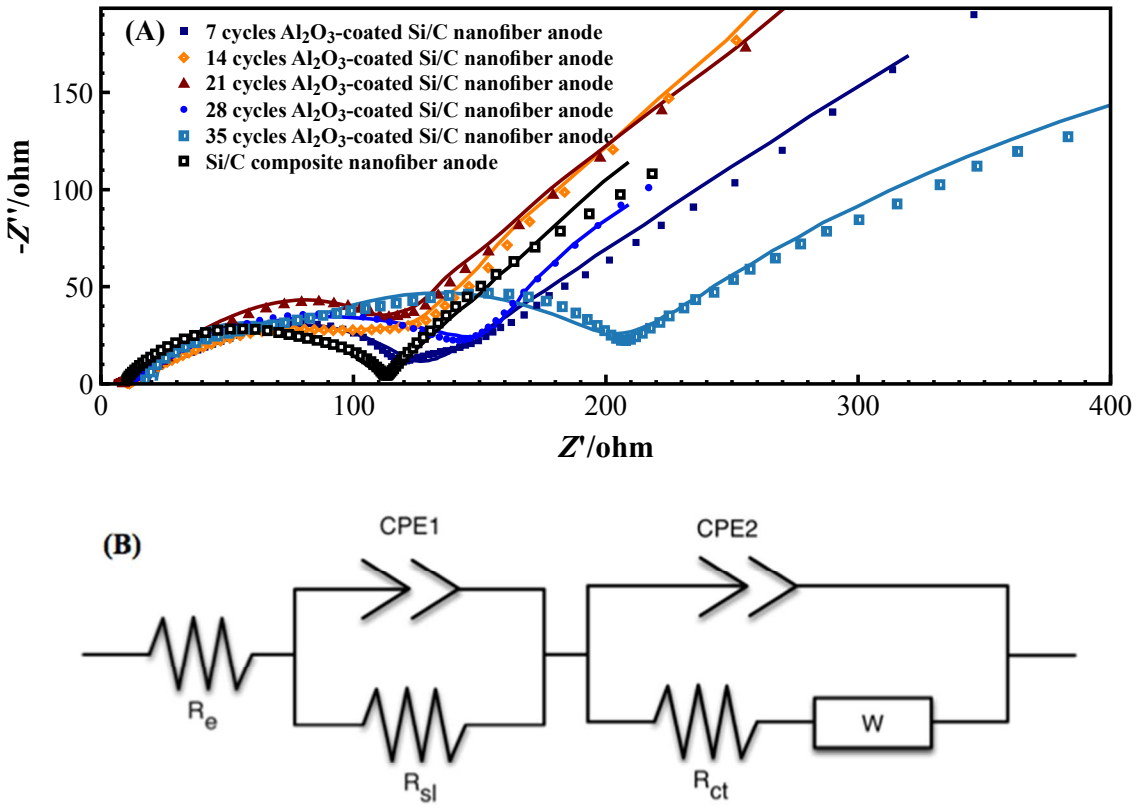

Figure 8. (A) Nyquist plots and (B) equivalent circuit of Si/C composite nanofibers and Al_2O_3-coated Si/C composite nanofibers. In (A), symbols show experimental data and solid lines are fitted curves.

Journal of Materials Chemistry A Accepted Manuscript

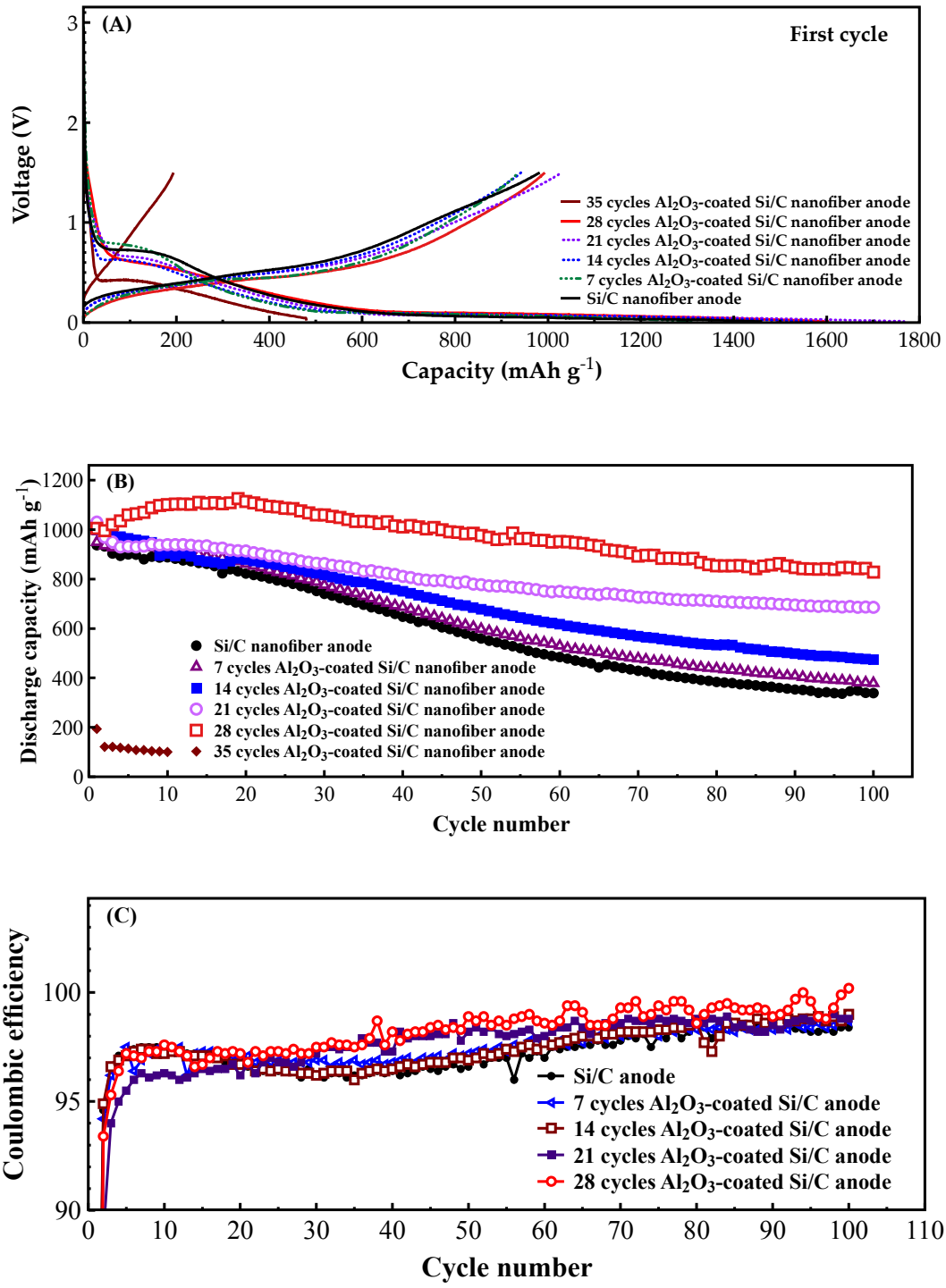

Figure 9. (A) Galvanostatic charge-discharge curves, (B) cycling performance, and (C) Columbic efficiencies of Si/C composite nanofibers and Al_2O_3-coated Si/C composite nanofibers.

Journal of Materials Chemistry A Accepted Manuscript

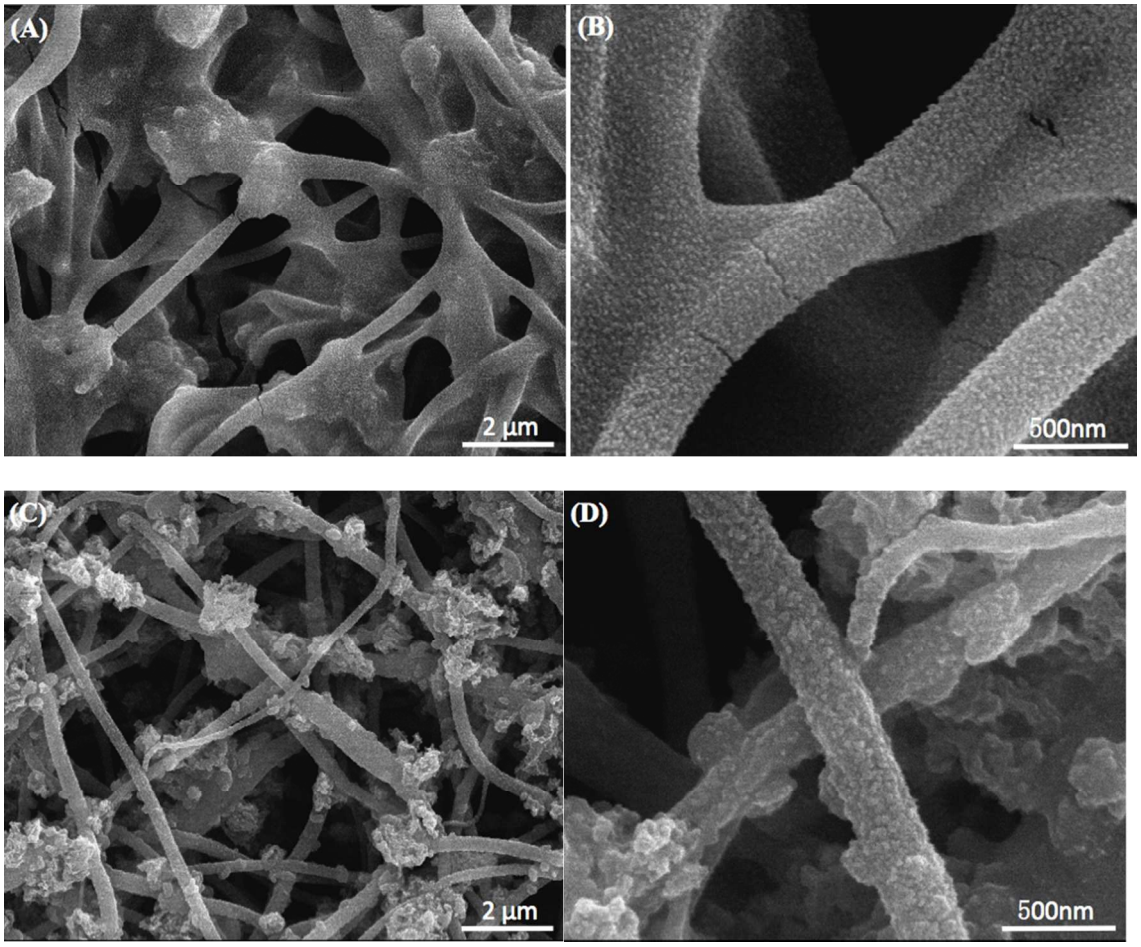

Figure 10. SEM images of (A, B) Si/C composite nanofibers and (C, D) Al_2O_3-coated Si/C composite nanofibers (ALD cycle number = 28) after 100 charge-discharge cycles at a constant current density of 50 mA g^{-1}.

Journal of Materials Chemistry A Accepted Manuscript

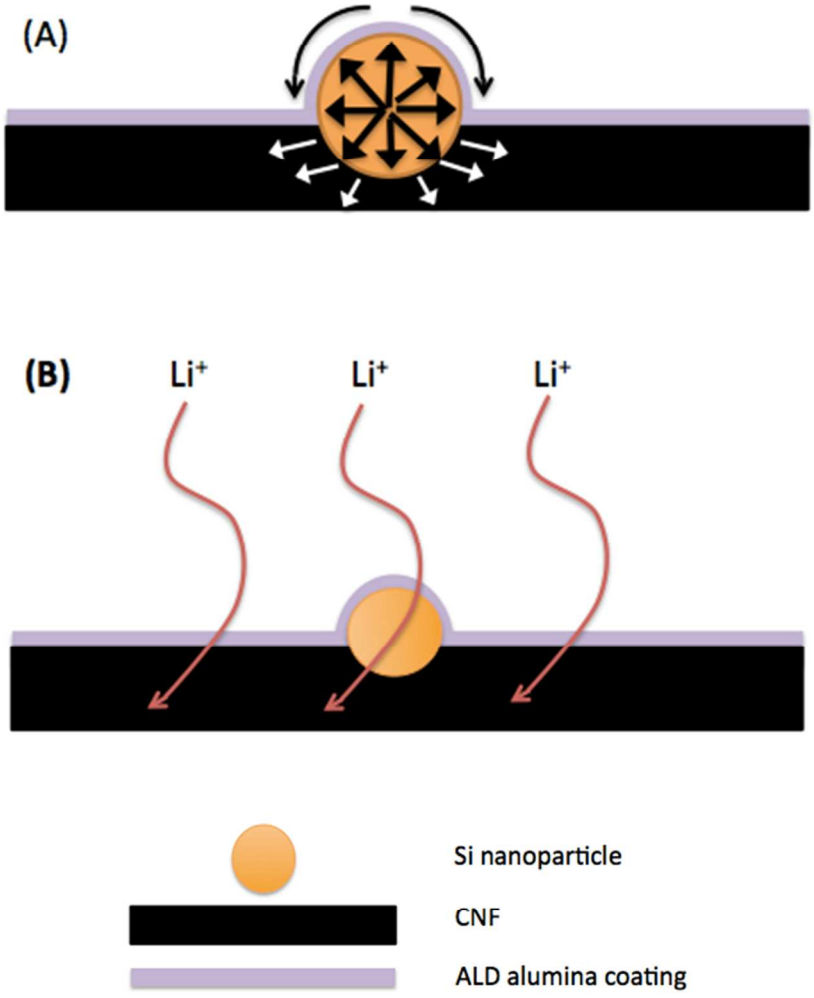

Figure 11. Schematic of (A) Physical/Mechanical, (B) Chemical protective effect.

Journal of Materials Chemistry A Accepted Manuscript

Table of Contents (TOC) Graphic

A free-standing, conductive and three-dimensional network of Al_2O_3-coated Si/C composite nanofibers is fabricated by a single-nozzle electrospinning and atomic layer deposition. The as-obtained Al_2O_3-coated Si/C composite nanofibers exhibit excellent electrochemical performance for applications as anode materials for lithium-ion batteries.

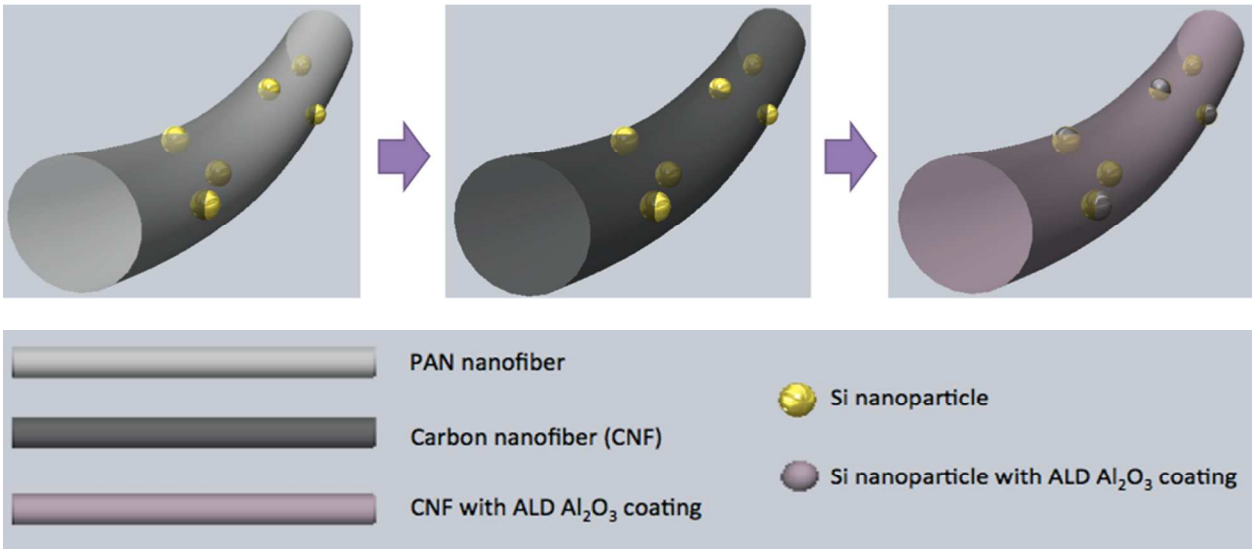

Journal of Materials Chemistry A Accepted Manuscript